Accepted Manuscript

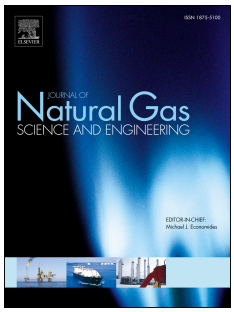

Enhancing coal seam gas using liquid CO_2 phase-transition blasting with cross-measure borehole

Guozhong Hu, Wenrui He, Miao Sun

PII: S1875-5100(18)30484-0

DOI: https://doi.org/10.1016/j.jngse.2018.10.013

Reference: JNGSE 2743

To appear in: *Journal of Natural Gas Science and Engineering*

Received Date: 16 July 2018

Revised Date: 12 October 2018

Accepted Date: 20 October 2018

Please cite this article as: Hu, G., He, W., Sun, M., Enhancing coal seam gas using liquid CO_2 phase-transition blasting with cross-measure borehole, *Journal of Natural Gas Science & Engineering* (2018), doi: https://doi.org/10.1016/j.jngse.2018.10.013.

Enhancing coal seam gas using liquid CO_2 phase-transition blasting with cross-measure borehole

Guozhong Hu [a], Wenrui He [b,] *, Miao Sun[a]

[a] School of Mines, Key Laboratory of Deep Coal Resource Mining, Ministry of Education of China, China University of Mining and Technology, Xuzhou, China

[b] College of resources and safety engineering, China University of Mining and Technology, Beijing, China

* Correspondence Email: 1522331579@qq.com (W. He); gzhu@cumt.edu.cn (G. Hu)

Abstract: The efficiency of gas drainage in deep coal seams is generally poor because of their typically low-gas permeability and high-geostress characteristics. Therefore, we conducted a test study on the permeability enhancement of cross-measure boreholes using liquid CO_2 phase-transition blasting (LCPTB) to identify an effective method for enhancing coalbed methane reservoir. Through a numerical simulation of LCPTB, the fracture propagation in the coal seam after blasting was analysed. Subsequently, a field test arrangement for boreholes of LCPTB was designed, and the range of enhanced permeability after blasting as well as the efficiency of gas drainage were investigated. The results indicate a significant increase in the permeability of the coal seam and the efficiency of gas drainage following LCPTB. The amount of gas extracted from the blast holes was 1.8–8 times greater than that extracted from boreholes without LCPTB. The practical spacing between boreholes was deemed to be 2.5–3 m. In addition, with decreasing measuring distance from the blast hole, the efficiency of LCPTB was improved by increasing the permeability of the coal mass surrounding the observation hole. The observation holes arranged around the blasting holes could increase the efficiency of gas drainage. In summary, this technology uses the energy released by LCPTB to increase the permeability of the coal surrounding the blast hole, and to displace methane in the coal seam, thereby improving the efficiency of gas drainage and providing economic and environmental benefits.

Keywords: gas drainage; liquid carbon dioxide; phase-transition blasting; enhancing coalbed methane

1 Introduction

The pre-drainage of coal seam gas is an effective method for controlling coal mine gas accidents. However, coal seams in many coal mines exhibit poor gas permeability, high ground stress, and poor coal seam gas drainage efficiency (Qian et al., 2007; Qin, 2008). It is thus necessary to obtain a safe and effective method of enhancing coal seam permeability and enable efficient coal seam gas drainage (Liang et al., 2014; Xie et al., 2013; Hu et al., 2009; Jiang et al., 2017; Yin et al., 2015 and Hu et al., 2015a). For improving the gas drainage effectiveness, a new technology using liquid CO_2 phase-transition blasting (LCPTB) is presented. It is different from chemical blasting, in that LCPTB technology utilizes the high-energy gas (Wu et al., 2018) generated by the instantaneous phase-transition of liquid CO_2 to impact the coal mass, causing it to break and generate numerous fractures to provide channels for gas desorption and migration. LCPTB technology is extremely safe,

and is utilised widely in enhanced coalbed methane (ECBM) reservoir.

LCPTB technology was first proposed by the British company, Carbon. Singh (Singh, 1998.) introduced the equipment structure and application of this technology, and Patrick (1995) summarised the advantages of CO_2 blasting relative to traditional chemical blasting. This blasting technology is simple to operate; as such, it is utilised widely in surface soil stripping (Viadanovic et al., 2011), tunnelling, and pipe cleaning (Spur et al., 1999). At the end of the 20th century, supercritical CO_2 was introduced to the coal industry and was found to yield good results in coal seam permeability enhancement (Moore, 2012; White et al., 2005; Hamelinck et al., 2001. Zhou et al., 2013; and Black et al., 2011). Sun et al. (2017) analysed the relationship among CO_2 gas pressures, time of action, coal strength and crack occurrence. Chen et al. (2017) obtained the effective permeability-increasing radius after LCPTB by field tests. Zhang et al. (2013) used LCPTB technology in the mining process of a fully mechanized mining face, and concluded that this technology can be used to cave coal efficiently. Sun et al. (2017) analysed the damage mechanism of supercritical CO_2 phase-transition blasting of coal seams. Liu et al. (2017) developed an LCPTB test for enhancing permeability in the LF mine in Guizhou. Wang et al. (2017) compared and analysed the failure and fracture characteristics of rock masses after hydraulic fracturing and critical CO_2 blasting. Sampath et al. (2017) reported that CO_2 gas exhibited obvious exchange and displacement effects with methane in coal seams. Vishal (2017) investigated the patterns of change in permeability after introducing CO_2 gas into coal seams. In summary, these studies revealed the mechanism of LCPTB in increasing the permeability of coal seams as well as some simple engineering attempts. However, studies regarding the enhancement of coal seam gas using LCPTB with cross-measure boreholes are scarce, although they are critical for perfecting and popularizing LCPTB-ECBM technology.

This paper investigates the influence radius of LCPTB by numerically analysing fracture propagation patterns following LCPTB of coal seams in the XDD coal mine of the Yangquan coal field, China. Engineering tests on cross-measure boreholes using LCPTB were subsequently developed and conducted, and the efficiency of coal seam gas drainage before and after blasting was investigated.

2 Simulation on fracture propagation patterns in coal seams after LCPTB

The aim of this simulation is to clarify the fracture propagation patterns following LCPTB in the #15 coal seam of the XDD coal mine, and to determine the permeability-increasing ranges of coal seams. This would provide insight into the rational arrangements of blasting holes for field tests.

2.1 Overview of study site

The study area pertaining to increasing the permeability of the coal seam using LCPTB is located between the 15405 and 15404 working faces of the XDD coal mine in the Yangquan coal field, China, as shown in Fig. 1. The intake and return airways of the 15405 and 15404 working faces were arranged in the #15 coal seam, as shown in Fig. 1a. The rock roadway in the floor was arranged in the rock stratum under the #15 coal seam between the 15404 intake and the 15405 return airways, as shown in Fig. 1b.

The average depth of the coal seam is 440 m. The initial gas content of the coal seam was 11.69 m^3/t, and the gas permeability coefficient was 0.0039 $m^2/MPa^2 \cdot d$; thus, it was classified as a coal seam with low gas permeability. The direct roof of the #15 coal seam is sandy mudstone, and the floor is soft mudstone. At the site of rock roadway in the floor, cross-measure boreholes were drilled to the intake airway of the 15404 working face and the return airway of the 15405 working face; subsequently, LCPTB was applied to enhance the permeability.

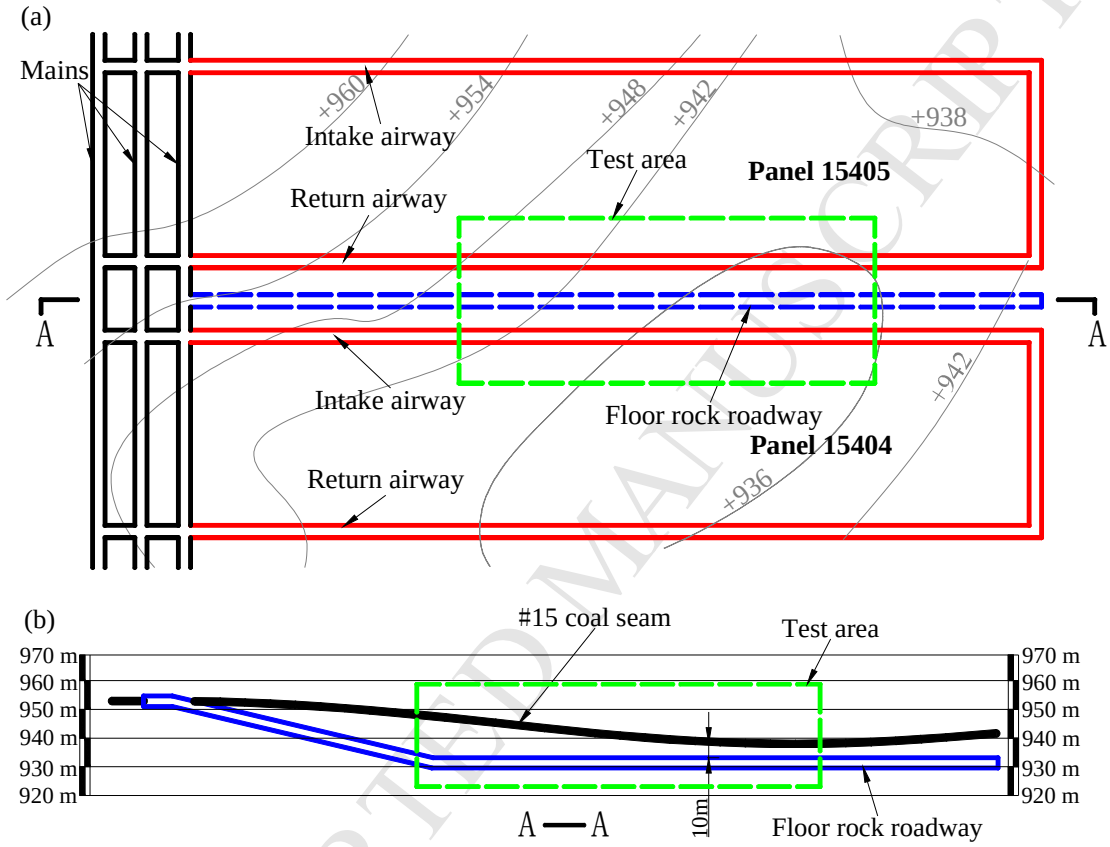

Fig.1. Testing site (a) top view; (b) profile

2.2 Physical and mechanical parameters of coal seam

Coal samples were drilled from the #15 coal seam to obtain parameters, which would be used in the numerical analysis. The physical and mechanical parameters of the coal samples were tested according to the industry standard DZ/T 0276.20-2015 (DZ/T 0276.19-2015, 2015). The coal density was obtained from literature (Robeck and Huo, 2016). The practical parameter setting is crucial to ensure the accuracy of the numerical analysis. Wang et al. (2003) suggested the elastic modulus and tensile strength of coal to be in the range of 0.1–0.25 times that of the laboratory values, whereas the elastic modulus and tensile strength of coal in this study were 0.25 times that of the laboratory tests. Meanwhile, Mohammad et al. (1997) suggested the Poission's ratio to be in the range of 1.2–1.4 times that of the laboratory values, whereas the Poission's ratio was 1.2 times that of the laboratory values in this study. The physical and mechanical parameters of coal are shown in Table 1.

Table 1. Physical and mechanical parameters of coal seam

Parameter	Density ρ (kg/m^3)	Tensile strength σ_t (MPa)	Elastic modulus E (GPa)	Poisson's ratio μ
Laboratory value	1050	2.16	5.2	0.25
Value for simulation	1050	0.54	1.3	0.3

2.3 Numerical analysis

The ANSYS-LS-DYNA software was used to study the fracture propagation in the coal seam after LCPTB. It can solve problems of highly nonlinear structural dynamics, including nonlinear dynamic shock problems such as explosion, collision, and metal forming. It is based on the Lagrange algorithm and contains both ALE and Euler algorithms.

2.3.1 Control equations

In the numerical analysis of plane stress and strain, the Griffith strength criterion was used to describe the coal body damage.

$$\begin{cases} (\sigma_1 - \sigma_3)^2 - 8\sigma_t(\sigma_1 + \sigma_3) = 0 \\ \sigma_1 + 3\sigma_3 \geq 0 \\ \sigma_3 = -\sigma_t \\ \sigma_1 + 3\sigma_3 < 0 \end{cases} \quad (1)$$

where σ_t is the tensile strength, σ_1 is the maximum normal stress, and σ_3 is the minimum normal stress.

As air was assumed to be an ideal gas, and linear solid elements were used in LS-DYNA, the air control equation is as follows:

$$p = (\gamma - 1)\frac{\rho}{\rho_0}E_0, \quad (2)$$

where γ is the ratio of specific heat, and was assumed to be 1.4 according to the literature (Schwer, 2010). ρ_0 is the initial density of air. The initial value of E_0 was given as 0.25 MPa according to Schwer, and an initial air temperature of 20°C was assumed.

The Jones Wilkins and Lee (JWL) equation of state (Eq. 3) was used to model the blasting process. The empirically derived model was developed from cylindrical explosive test data and is utilised widely owing to its simplicity and computational efficiency (Courtney and Tarefder, 2017). The LS-DYNA high explosive burn (HEB) material model was used with the JWL equation of state. The HEB model describes the pressure in the high explosive material, utilizes a burn fraction during detonation simulations to calculate the amount of reacted explosive material and controls the release of chemical energy during the detonation (Hallquist, 2012). An LS-DYNA null material and an ideal gas linear polynomial equation of state were used to model the air in the calculations.

$$\mathrm{p} = \mathrm{A}\left(1 - \frac{\omega}{R_1 V}\right)e^{-R_1 V} + B\left(1 - \frac{\omega}{R_2 V}\right)e^{-R_2 V} + \frac{\omega E}{V}, \quad (3)$$

where p is the blast pressure; V is the current relative volume (volume of material at pressure p divided by the initial volume of unreacted explosive.); E is the specific internal energy (internal energy per initial volume); A, B, R_1, R_2, and ω are the JWL coefficients based on explosive testing.

2.3.2 Simulation model, initial and boundary condition

The width and height of the model were 30 m respectively. A blasting hole was located in the centre of the model, and its diameter was 0.09 m. The CO_2 blasting tube was located at the centre of the blasting hole. The medium between the CO_2 blasting tube and the blasting hole was air. The four sides of the model were set as non-reflecting boundaries, and the borehole wall was set as a free boundary, as shown in Fig. 2.

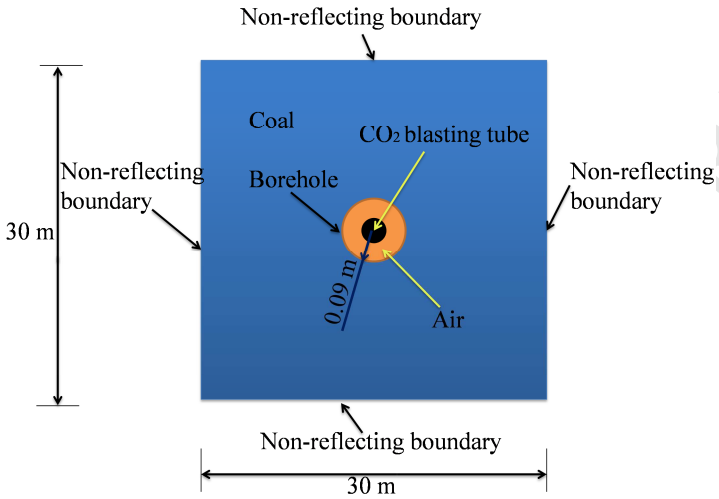

Fig. 2. Numerical model

2.3.3 Model verification

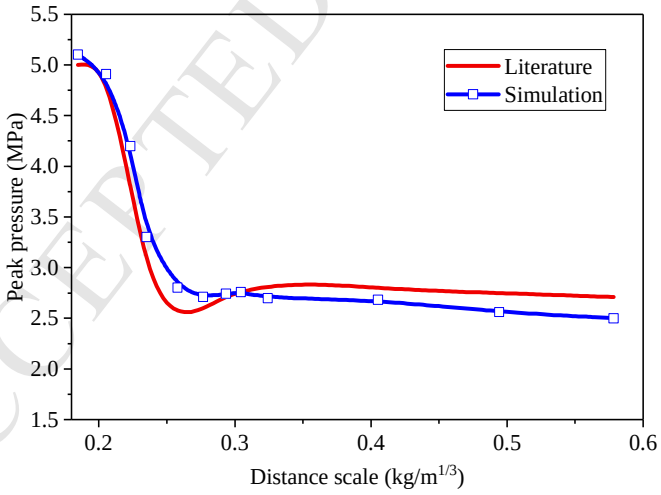

Fig.3. Numerical result verification

In this study, the validity and accuracy of the model were verified by comparing different scale distances (kg/m$^{1/3}$) based on numerical analysis parameters in the literature (Han and Liu, 2015). The scale distance is the ratio of the distance from the explosive to the blasting medium and the amount of explosives. The numerical results are verified, as shown in Fig. 3. The numerical analysis results are close to those in the literature, indicating the reliability and accuracy of the model in this study.

2.3.4 Calculation of explosive yield

The energy released in the phase-transition device during liquid CO_2 fracturing can be approximated using the following equation (Li and Wang, 2010),

$$E_g = \frac{pV}{k-1}\left[1 - \left(\frac{101325}{p}\right)^{\frac{k-1}{k}}\right], \quad (4)$$

where E_g is the blasting energy of the gas in J, V is the volume of the container in m^3, p is the absolute pressure in the container in Pa, and k is the adiabatic index, which is 1.295 for CO_2.

The MZL-200 liquid CO_2 explosive fracturing device was used in the current engineering test of the cross-measure borehole using LCPTB. The discharge pressure of its constant-pressure shear plate was approximately 200 MPa, the volume of the reservoir was 2.25 L, and the amount of moveable liquid CO_2 was 1 kg. From (Eq. 4), the energy, E_g, released by a single MZL-200 liquid CO_2 explosive fracturing device after detonation was calculated to be 1254.58 kJ. The energy E_g released by the MZL-200 liquid CO_2 explosive fracturing device was converted to the TNT equivalent W_{TNT} by using the following equation (Dong et al., 2014),

$$W_{TNT} = \frac{E_g}{Q_{TNT}}, \quad (5)$$

where W_{TNT} is the TNT equivalent of the liquid CO_2 fracturing device in kg and Q_{TNT} is the explosive yield of 1 kg TNT at 4250 kJ/kg.

From (Eq. 5), the TNT equivalent of a single MZL-200 liquid CO_2 explosive fracturing device after detonation was calculated to be 0.295 kg TNT. This study simulated the use of five CO_2 explosive fracturing devices, which is equivalent to using of 1.475 kg TNT.

2.4 Numerical simulation results

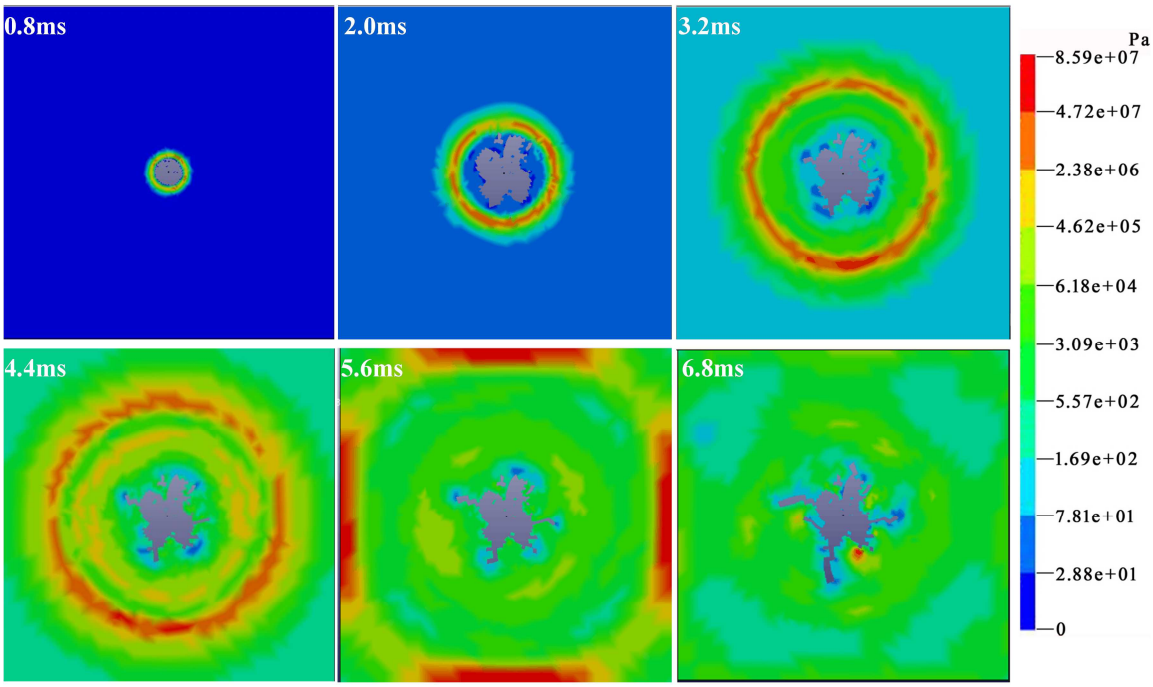

Fig. 4. Stress wave propagation diagram

Figure 4 shows the process of stress wave propagation in the coal seam after LCPTB. At 0.8–5.6 ms, the stress produced by LCPTB propagated gradually from the borehole orifice towards the deeper coal seam. This caused the compression of deep coal formations located far from the orifice. It also increased the stress, where the largest stress waves were located in the centre of the area of increased stress (approximately 8.59×10^7 Pa). At 5.6–6.8 ms, the strength of the stress waves weakened gradually with continued forward propagation, and the stress in the coal formation decreased. At 6.8 ms, the stress in the area surrounding the fracture was fully released (at 0–78.1 Pa), and no further propagation of the coal seam fracture occurred. However, owing to the mutual extrusion effect of the coal matrix after blasting, an amount of residual stress with a maximum value of 6.18×10^4 Pa remained in the coal seam.

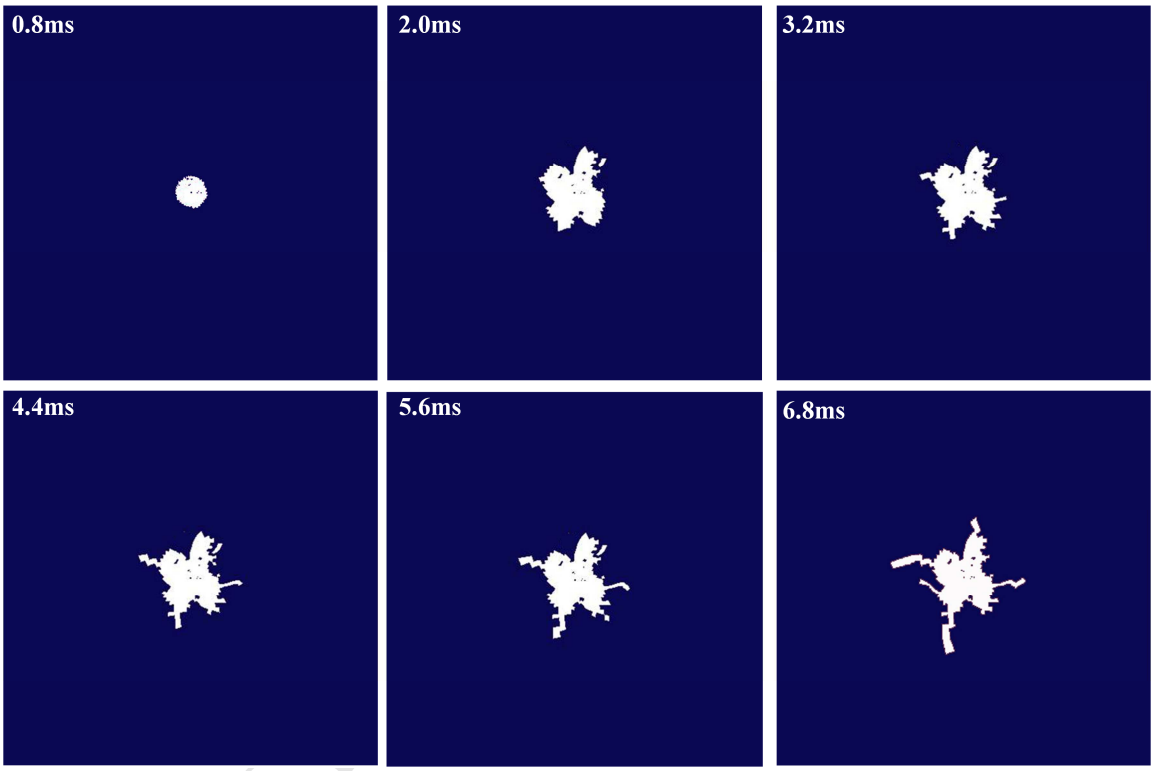

Fig. 5. Coal seam fracture propagation process

Figure 5 shows the process of fracture development and propagation in the coal seam after LCPTB. As shown, the high-stress waves produced after LCPTB generated an impact that exhibited a compressive effect on the coal formation. At 0–0.8 ms, the coal formation surrounding the blast hole underwent an extrusive force under the compressive effect of the stress wave, thereby causing a compressive fracture that gradually formed a regular, round crush zone. At 0.8–2.0 ms, the range of the coal formation fracture propagated further and formed an even larger irregular fracture development zone. At 2.0–3.2 ms, the LCPTB energy decreased, and the coal formation crush zone, which is primarily related to the compressive fracture, gradually stopped developing. The fracture subsequently expanded rapidly with a propagation speed of approximately 1.25 m/ms under the action of gases

related to the detonation at 3.2–5.6 ms. The fracture propagation speed was reduced significantly, and its extension speed was reduced rapidly from 1.25 m/ms to 0.12 m/ms. At 5.6–6.8 ms, the energy decay from LCPTB was reduced, the coal formation stabilised after stress redistribution, and fracture propagation terminated. Therefore, after LCPTB, a regular circular crush zone forms in the coal formation surrounding the blast hole, and an irregular fracture development zone develops from the inside out. The coal in the regular circular crush zone exists in a crushed form, and the radius of this area was approximately 2.5 m for this mine. Six fractures of lengths of 2.5–3 m existed in the irregular fracture development zone, two fractures of lengths of 3–5 m, and two fractures of lengths of 5–6.5 m. Overall, the numbers of fractures with lengths between 3 m and 6.5 m after blasting was small, and the direction of fracture propagation could not be determined easily; therefore, it is difficult to form a wide range of connectivity when the gas drainage holes are deployed in a radius of 3–6.5 m around the coal formation. Therefore, the effective influence radius of LCPTB in the 15404 site of the XDD mine was approximately 2.5–3 m.

3 Methodology

3.1 Equipment system

(1) Injection device

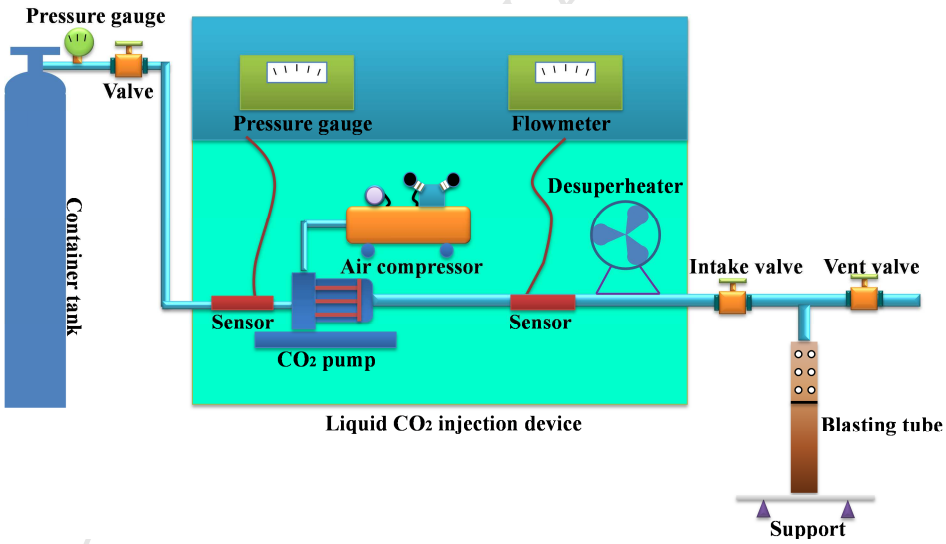

Fig. 6. Liquid CO_2 injection device

Figure 6 shows the liquid CO_2 injection device that consists primarily of a container tank, air compressor, CO_2 pump, desuperheater, and flowmeter. The air compressor provides pressure to the CO_2 pump that draws liquid CO_2 from the container tank and delivers it to the blasting tube. The flowmeter monitors the flow of liquid CO_2 in the tube, and the pressure gauge monitors the pressure of liquid CO_2 in the tube. The desuperheater is used to lower the temperature of liquid CO_2 in the tube, thereby maintaining it in the liquid phase.

(2) Fracturing device

The liquid CO_2 fracturing device is composed primarily of a push rod, injector connector, heater,

reservoir, constant-pressure shear plate, and release tube, as shown in Fig. 7. The heater is used to heat liquid CO_2 in the reservoir, thereby converting it into the gaseous phase. Subsequently, the constant-pressure shear plate ruptures when the expansion pressure generated by the gas exceeds its anti-shear strength. The release tube is a porous steel tube; the size and position of the pores control the positions at which pressurised gas is applied.

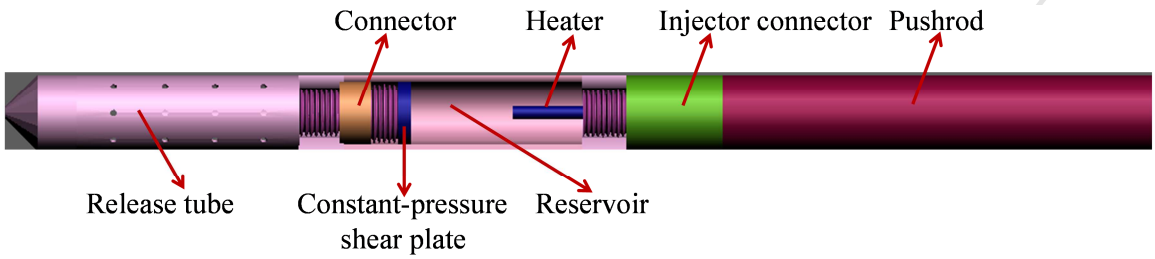

Fig. 7. Liquid CO_2 fracturing device

(3) Propulsion machine

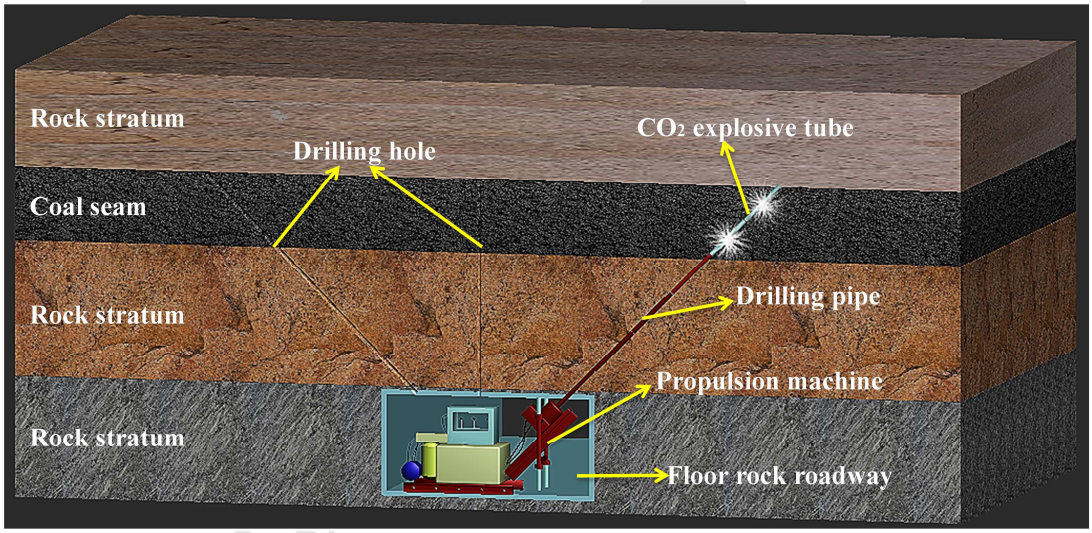

Fig. 8. Propulsion machine

To transport the CO_2 blasting tubes to the coal seam whose permeability must be increased, three steps are required. First, a rock roadway in the floor of the coal seam was drilled, and the drilling holes were drilled from the floor rock roadway to the upper coal seam. Subsequently, the propulsion machine was driven into the floor rock roadway, and the CO_2 blasting tubes were pushed to the coal seam by the propulsion machine through the drilling holes. After the CO_2 blasting tubes were exploded, the CO_2 blasting tubes were exited from the drilling holes, as shown in Fig. 8.

3.2 Basic principles

The critical temperature of the liquid CO_2 phase-transition is 31°C, and the critical pressure is 7.39 MPa. When the temperature is higher than the critical temperature, regardless of the amount of pressure,

the CO_2 cannot be liquefied (Hou et al., 2006). The LCPTB process occurred for approximately 20 ms, the instantaneous pressure of the CO_2 gas reached 140–276 MPa, and the gas expansion volume of the liquid CO_2 after blasting was approximately 600 times that of the liquid. Before blasting, the CO_2 in the liquid storage pipe is in a high-pressure liquefaction state and belongs to a permanent cryogenic liquid. After the heater is turned on, the temperature of the liquid CO_2 in the liquid storage tube increases, and part of the liquid CO_2 undergoes a phase change and converts into gas; simultaneously, the temperature and pressure inside the tube are increased. When the temperature and pressure reach a certain level, the CO_2 in the liquid storage tube is in the supercritical state of gas–liquid coexistence. When the pressure in the CO_2 reservoir reaches the pressure to break the constant-pressure shear plate, the high-pressure CO_2 gas is flushed out and impacts on the coal body around the blasting holes. The primary source of energy is the physical explosion energy in this process. When CO_2 is converted from liquid to gaseous, it absorbs a large amount of heat energy and reduces the ambient temperature around the borehole. Simultaneously, the blasting process is safe and reliable, and the risk of gas explosion is none because CO_2 is an inert gas.

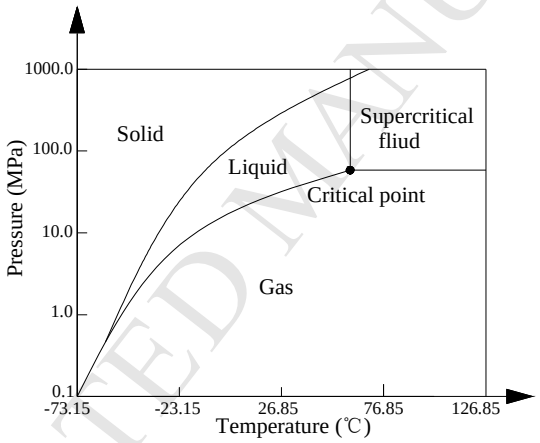

Fig. 9. The phase of CO_2 (Liu et al., 2013)

In the LCPTB process, the liquid CO_2 first transitions into CO_2 gas in the reservoir. When it acts on the coal and enters the fracture of the coal body, it becomes a high-energy CO_2 gas. This CO_2 gas is used as a blasting medium to break the rock and coal. The blasting fracturing process can be divided into two stages: the initial high-pressure impact compression stage; the middle and late high-energy gas fracturing stage. The former is the initial high-pressure impact and compression failure stage, whereas the latter is the high-energy gas coal-splitting stage in the middle and late periods. The high-energy CO_2 gas generated in the initial stage of the blasting impacts the coal around blasting hole. Under compression, the coal around the blasting hole breaks down, forming a crush zone and generating a stress wave to propagate far away. Subsequently, the high-energy gas enters the coal body fracture to split the coal body and further aggravate fracture propagation and damage (Du et al., 2012). Additionally, the coal exhibits a higher sorption capacity of CO_2 than methane; therefore, CO_2 can partially occupy methane sorption sites through high-pressure injection and displace methane from the coal formation, thus increasing the gas drainage efficiency from coal seams.

3.3 Program for test boreholes deployment

3.3.1 Test boreholes design

Based on the above numerical simulation results and the geological conditions of site 15404, a borehole arrangement for the test region was formulated, as shown in Fig. 10. The borehole deployment used the following three programs with the associated conditions: (Program 1) using a row spacing of 5 m between gas drainage holes, a spacing of 2 m between adjacent drainage boreholes, and the blast hole positioned at the midpoint between the two groups of drainage holes (observation holes); (Program 2) using a row spacing of 3 m between gas drainage holes, a spacing of 2 m between adjacent drainage boreholes, and the blast hole positioned at the midpoint between the two groups of drainage holes (observation holes); (Program 3) using a row spacing of 10 m between boreholes, no gas drainage surrounding the blast hole, and boreholes designated as B_9–B_{14}. In these programs, each group of drainage holes (observation holes) was composed of two adjacent rows of boreholes in a fan-shaped arrangement, with a total of seven boreholes in each group.

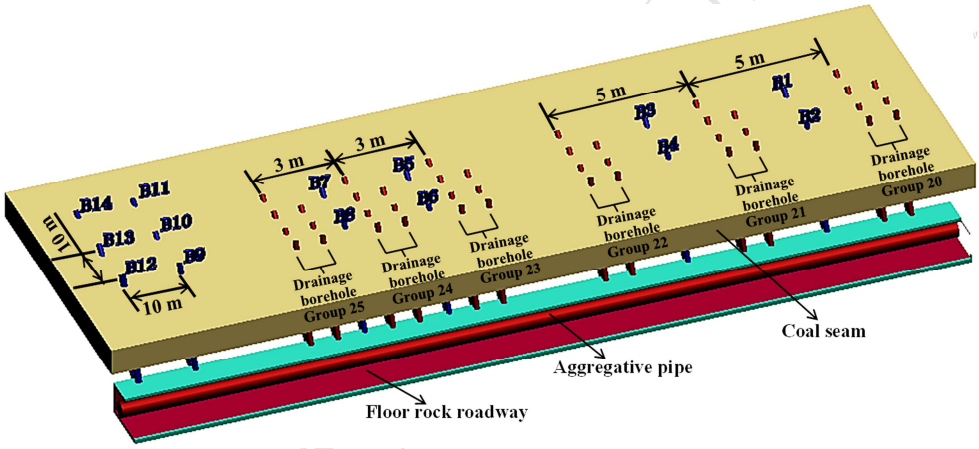

Fig. 10. Schematic diagram of borehole deployment

3.3.2 Connectivity of borehole flowmeters

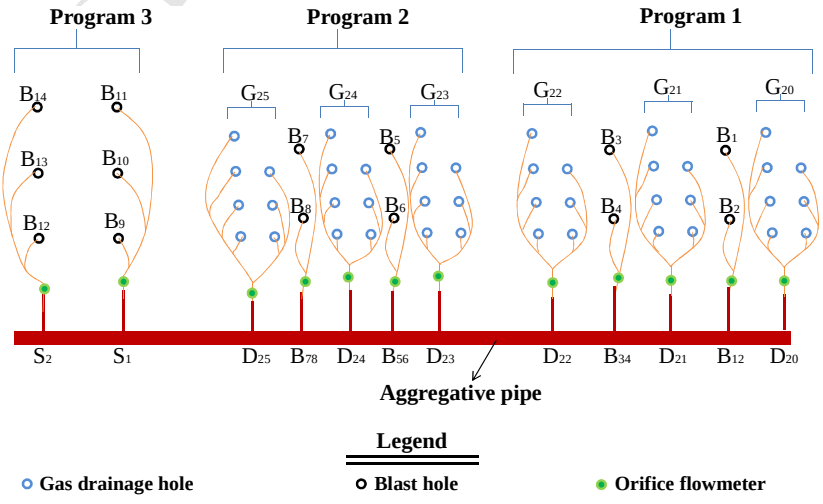

Fig. 11. Connectivity of borehole flowmeters

Gas drainage efficiency investigations consist primarily of determining the amount and concentration of the drained gas. Figure 11 shows the connectivity of borehole flowmeters. Among them, the B_{12}, B_{34}, B_{56}, B_{78}, S_1, and S_2 groups are the flowmeters of the blast holes, and D_{20}, D_{21}, D_{22}, D_{23}, D_{24}, and D_{25} groups are the flowmeters of the drainage holes (observation holes).

4 Results and discussion

4.1 Gas drainage results of blast holes

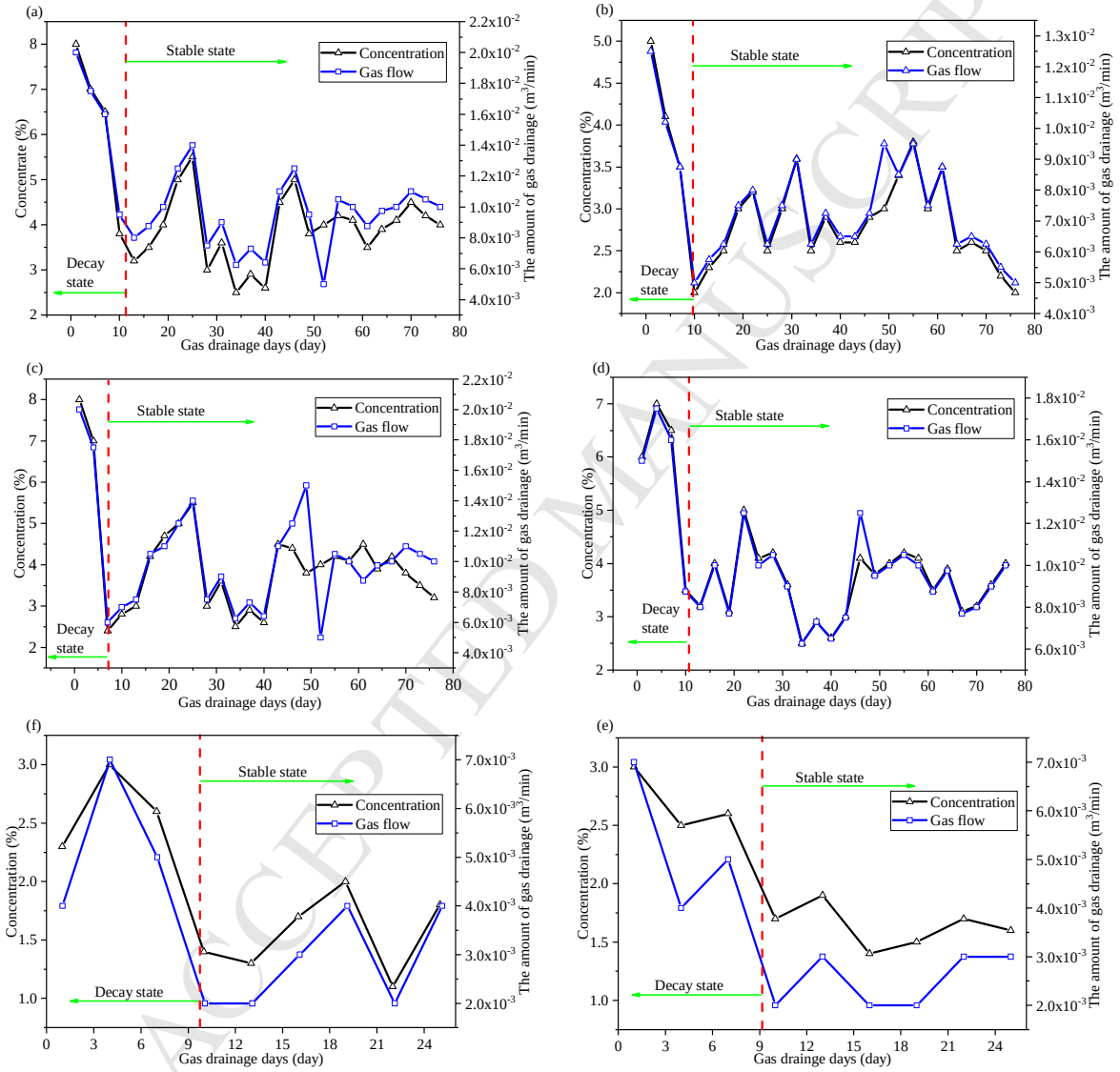

Fig. 12. Gas drainage efficiency of blast holes

(a) group B_{12} blast holes, (b) group B_{34} blast holes, (c) group B_{56} blast holes, (d) group B_{78} blast holes, (e) group S_1 blast holes and (f) group S_2 blast holes

Table 2. Average amount of gas drainage in the stable production period of blasting holes after blasting

Group of blast holes	B_{12}	B_{34}	B_{56}	B_{78}	S_1	S_2
The average amount of gas drainage (m^3/min)	1.04×10^{-2}	7.45×10^{-3}	9.98×10^{-4}	9.93×10^{-3}	3.6×10^{-3}	3.4×10^{-3}

Figure 12 and Table 2 show that the amount and concentration of gas drained from the blast holes were both maintained at a high level after LCPTB. However, because the coal seam gas in the range of influence of the blast was fully desorbed and extracted, the amount of gas drainage occurring in the coal seam decreased gradually, approximately 10 d following blasting and reached a stable state thereafter. The average amounts of gas drained in the following boreholes were 0.0104 m^3/min from the B_{12} blast group, i.e. 8-fold that of the boreholes not using LCPTB; 0.00745 m^3/min from the B_{34} blast hole group, i.e. 5.7-fold that of the boreholes not using LCPTB; 0.000998 m^3/min from the B_{56} blast hole group, i.e. 7.7-fold that of boreholes not using LCPTB; 0.00993 m^3/min from the B_{78} blast hole group, i.e. 7.6-fold that of boreholes not using LCPTB; 0.0036 m^3/min from the S_1 blast hole group, i.e. 1.9-fold that of boreholes not using LCPTB; 0.0034 m^3/min from the S_2 blast hole group, i.e. 1.8-fold that of boreholes not using LCPTB.

The results of the tests indicate that the gas drainage efficiencies from the blast holes created in Programs 1 and 2 were similar, and that a 5.7–8-fold increase in gas drainage amount occurred after blasting. However, Program 3 only provided a 1.8- and 1.9-fold increase in the blast hole gas drainage amount, which are far lower than those of Programs 1 and 2. A possible reason for this result is that the blast hole spacing in the Program 3 test area was relatively large; therefore, the energy produced from LCPTB was propagated into the coal formation surrounding the blast hole, thereby compressing the coal formation strongly. No other gas drainage holes were deployed around the blast hole; thus, no surfaces were available to provide an expansion space for the extruded coal, thereby preventing the stress from being fully released. This implied that the fractures produced by the blast could not communicate with the further depths of the coal formation, thus resulting in the reduced effective range of permeability enhancement by blasting, and a large decrease in the amount of drained gas.

4.2 Gas drainage results of observation holes

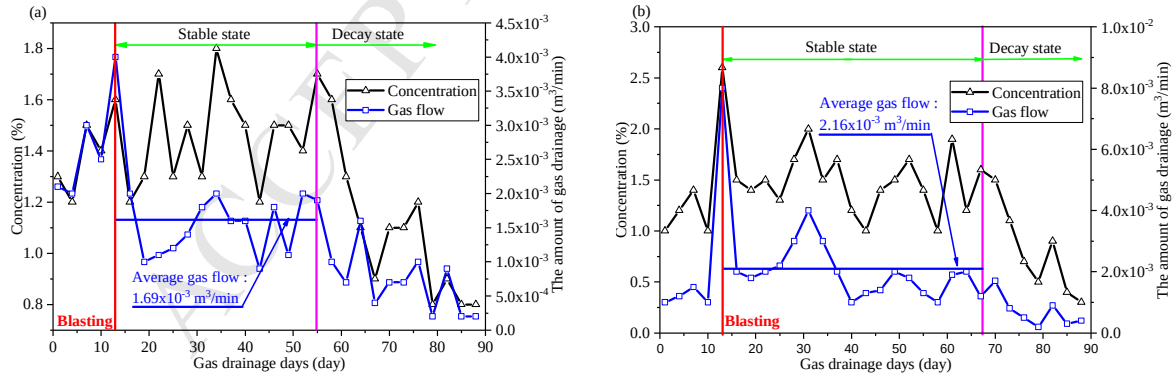

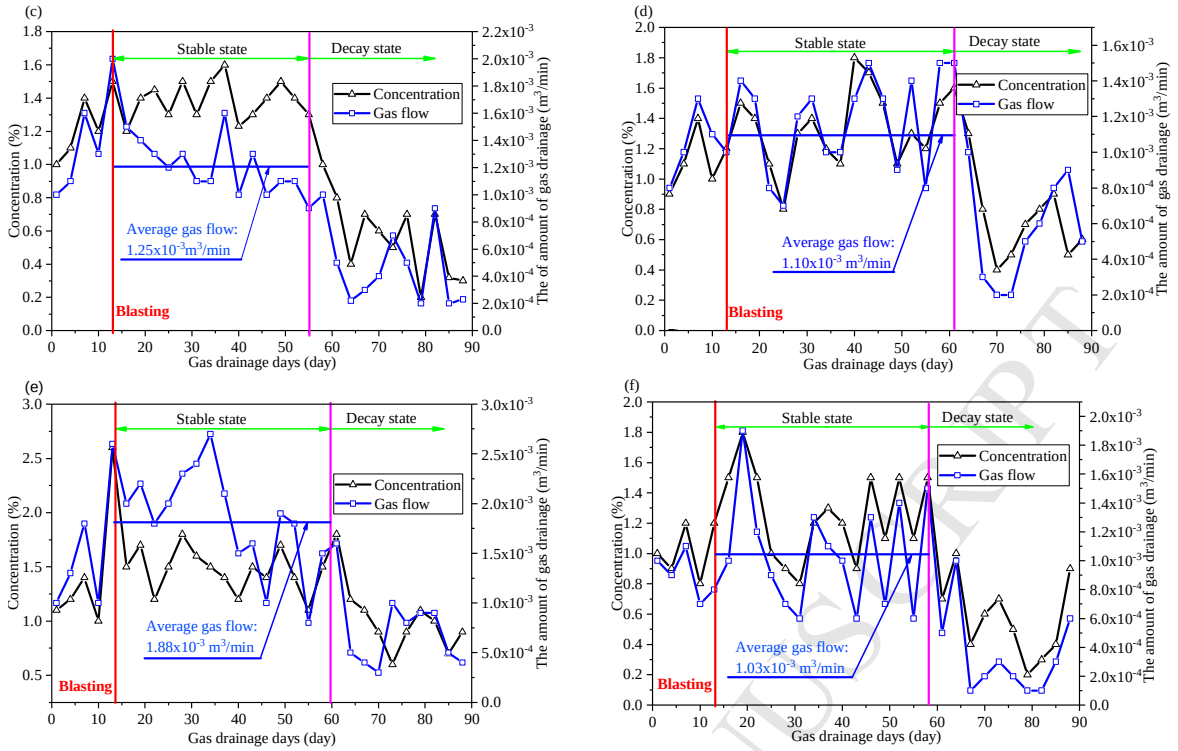

Fig. 13. Gas drainage efficiency of observation holes after blasting

(a) group D_{25} observation holes, (b) group D_{24} observation holes, (c) group D_{23} observation holes, (d) group D_{22} observation holes, (e) group D_{21} observation holes and (f) group D_{20} observation holes

Table 3. Average amount of gas drainage in the stable production period of gas drainage holes after blasting

Group of observation holes	D_{25}	D_{24}	D_{23}	D_{22}	D_{21}	D_{20}
The average of gas drainage (m^3/min)	1.69×10^{-3}	2.16×10^{-3}	1.25×10^{-3}	1.10×10^{-3}	1.88×10^{-3}	1.03×10^{-3}

Figure 13 shows the gas drainage efficiency of the observation holes after blasting using Programs 1 and 2; Table 3 shows the average amount of gas drainage in the stable production period of gas drainage holes after blasting. As shown, the concentrations and amounts of gas drained after LCPTB increased to a certain extent and subsequently reached a stable state. With the increased gas drainage time, the concentrations and amounts of drained gas in the observation holes decrease gradually, and gas drainage enters a decay state. The gas drainage amount in the observation holes in the D_{21} group of Program 1 was higher than that for the observation holes in the D_{20} and D_{22} groups; the gas drainage amount in the observation holes in the D_{24} group with Program 2 was higher than that for the observation holes in the D_{23} and D_{25} groups. This is primarily because the observation holes in the D_{21} and D_{24} groups were deployed between two rows of blast holes; thus, they experienced the equivalent effect of two explosions, thus resulting in the relatively higher development of coal formation fractures surrounding the borehole, and a higher increase in permeability than the other observation holes.

In addition, the test results show that the stable-state duration of gas drainage in the observation holes with Program 1 and Program 2 were generally similar. The average gas drainage amount in the observation holes in the D_{24} group in Program 2 was 2.16×10^{-3} m^3/min, which was larger than that of the observation holes in the D_{21} group in Program 1 (average gas drainage amount of 1.88×10^{-3}

m^3/min); the average gas drainage amounts in the observation holes in the D_{23} and D_{25} groups in Program 2 were 1.69×10^{-3} m^3/min and 1.25×10^{-3} m^3/min, respectively, which was larger than those of the observation holes in the D_{20} and D_{22} groups in Program 1 (average gas drainage amounts of 1.10×10^{-3} m^3/min and 1.03×10^{-3} m^3/min, respectively). Comprehensively, the gas drainage efficiency of Program 2 (spacing of 3 m between observation holes) was superior to that of Program 1 (spacing of 5 m between observation holes); however, the difference was small. This indicates that the range of permeability enhancement from LCPTB in the test region was greater than 2.5 m, which is consistent with the numerical simulation results presented previously. In addition, the numerical simulation yielded a coal formation fracture zone radius of approximately 2.5 m after blasting. The deployment of gas drainage boreholes inside the fracture zone would lead to borehole collapse during blasting, thereby affecting gas drainage. Therefore, a spacing of 2.5–3 m is considered to be reasonable between gas drainage holes and the blast hole in the test region used in the present study.

5 Conclusions

(1) The technology employed in this study revealed the fracture propagation pattern in coal seams after tests on cross-measure boreholes using LCPTB. The radius of the regular crush zone surrounding the blast hole was approximately 2.5 m, and most fractures in the irregular fracture zone were distributed within a radius of 2.5–3 m from the borehole. The effective influence radius of LCPTB in the test region was therefore approximately 3 m.

(2) After LCPTB, the amount of gas drained from the blast hole was 1.8–8-fold higher than that in the boreholes without LCPTB. This indicated that LCPTB could increase the permeability and gas drainage efficiency in coal seams. In addition, the increasing efficiency of permeability from LCPTB was enhanced because of the arrangement of the observation holes around the blast hole.

(3) Various spacings were used between the observation holes and the blast hole for LCPTB, and certain differences were shown in gas drainage efficiencies between the observation holes. With the decreased spacing of the observation holes, the permeability enhancement by LCPTB increased in the coal formations surrounding the observation holes. We found that the practical spacing between the blast hole and observation holes should be 2.5–3 m in the test region.

(4) Cross-measure boreholes using LCPTB technology can fully utilise the energy released from CPTB, thereby increasing the gas permeability of coal mass surrounding the blast hole, displacing methane from the coal seam, and increasing the gas drainage efficiency in the coal seam. This method would thus yield significant economic and environmental benefits.

Acknowledgments

This work was supported by the Independent Innovation Project of “Double-First Class” Construction (2018ZZCX08).

References

Black D.J., Aziz T., Ren T., 2011. Enhanced gas drainage from undersaturated coal bed methane reservoirs, 3rd Asia Pacific Coalbed Methane Symposium, Brisbane, Australia. 118-126.

Chen H.D., Wang Z.F., Chen X.E., Chen X.J., Guo L.G., 2017. Increasing permeability of coal seams using the phase energy of liquid carbon dioxide, Journal of CO_2 Utilization. 19, 112-119.

Courtney L.B., Tarefder R.A., 2017. Evaluation of appropriate material model in LS-DYNA for MM-ALE finite element simulations of small-scale explosive airblast tests on clay soils, Indian Geotechnical Journal. 47(2), 173-186.

Dong Q.X., Wang Z.F., Ha Y.B., 2014. Research on TNT equivalent of liquid CO_2 phase-transition fracturing, China Safety Science Journal. 24, 84-88.

Du Y.K., Wang R.H., Ni H.J., 2012. Determination of rock breaking of high-pressure supercritical CO_2 jet, Journal of Hydrodynamics. 24(4), 554-560.

DZ/T 0276.19-2015, 2015. Regulation for testing the physical and mechanical properties of rock-Part 20: Test for determing the strength of rock in triaxial compression, People's Republic of China Geological Minerals Standard.

Hallquist J.O., 2012. LS-DYNA theoretical manual, Livermore Software Technology Corporation, Livermore.

Hamelinck C.N., Schreurs H., Faaij A.P.C., 2001. Potential for CO_2 sequestration and enhanced coalbed methane production in the Netherlands, Netherlands Agency Energy Environment. 2229-2232.

Han Y.Z., Liu H.B., 2015. Finite element simulation of medium-range blast loading using LS-DYNA, Shock & Vibration. 2015(2), 1-9.

Hou G.W., Ding X.W., Chen Y.Z., 2006. Study on heat transfer characteristics of supercritical CO_2, Chemical Equipment Technology. 27, 25-30.

Hu G.Z., Xu J.L., Ren T., Gu C.X., Qin Wei, Wang Z.W., 2015a. Adjacent seam pressure-relief gas drainage technique based on ground movement for initial mining phase of longwall face, International Journal of Rock Mechanics and Mining Science. 77, 237–245.

Hu G.Z., Wang H.T., Fan X.G., Yuan Z.G., Hong S., 2009. Mathematical model of coalbed gas flow with Klinkenberg effects in multi-physical fields and its analytic solution, Transport Porous Media. 76(3), 407–420.

Jiang C.B., Duan M.K., Yin G.Z., Wang J.G., Lu T.Y., Xu J., Zhang D.M., Huang G., 2017. Experimental study on seepage properties, AE characteristics and energy dissipation of coal under tiered cyclic loading, Engineering Geology. 221, 114-123.

Li W.W., Di G., Wang R.X., 2010. Analysis of a liquid CO_2 tank explosion on a ship, Safety and Environmental Engineering. 17, 95-99.

Liang B.,Yuan X.P., Sun W.J., 2014. Seepage coupling model of in-seam gas extraction and its applications, Journal of China University of Mining and Technology. 43(2), 208-213.

Liu G.Q., Ma L.X., Xiang S.G., 2013. Chemical and chemical data sheet, Chemical Industry Press.

Liu Y.L., Zhu H.Q., Huang S.G., 2017. Application of CO_2 blasting permeability improvement technology in gas pre-drainage test, Chemical Engineering Transactions. 59, 109-114.

Mohammad N., Reddish D.J., and Stace L.R., 1997. The relation between in situ and laboratory rock properties used in numerical modelling, International Journal of Rock Mechanics and Mining

Science. 34(2), 287-297.

Moore T.A., 2012. Coalbed methane: a review, International Journal of Coal Geology. 101, 36-81.

Patrick V., 1995. CO_2 blasting in Europe, Nuclear Engineering International. 40(448), 43-45.

Qian M.G., Miao X.X., Xu J.L., 2007. Green mining of coal resources harmonizing with environment, Journal of China Society. 32(1), 1-7.

Qin Y., 2008. Mechanism of CO_2 enhanced CBM recovery in China: a review, Journal of China University of Mining and technology. 18(3), 406-412.

Robeck E., Huo D., 2016. A more accurate method for estimating in situ coal density and mineral matter from ash and specific energy determinations, International Journal of Coal Geology. 168, 237-252.

Sampath K.H.S.M., Ranjith P.G., Matthai S.K., Rathnaweera T., Zhang G., Tao X., 2017. CH_4-CO_2 gas exchange and supercritical CO_2 based hydraulic fracturing as CBM production-accelerating techniques: A review, Journal of CO_2 Utilization. 22, 212-230.

Singh S.P., 1998. Non-explosive applications of the PCF concept for underground excavation, Tunneling and Underground Space Technology. 13(3), 305-311.

Spur G., Uhlmann E., Elbing F., 1999. Dry-ice blasting for cleaning: Process, optimization and application, Wear. 233-235, 402-411.

Sun W.B., Wang Y., 2017. Numerical simulation of rock fracturing by carbon dioxide phase-transition, 51st US Rock Mechanics/Geomechanics Symposium. 3, 1962-1967.

Sun K.M., Xin L.W., Wang T.T., Wang J.Y., 2017. Simulation research on law of coal fracture caused by supercritical CO_2 explosion, Journal of China University of Mining and Technology. 46(3), 502-506.

Schwer L., 2010. A Brief Introduction to coupling load blast enhanced with Multi-Material ALE: the best of both worlds for air blast simulation, LS-DYNA Forum, Bamberg, Germany.

Viadanovic N., Ognjanovic S., Ilincic N., 2011. Application of unconventional methods of underground premises construction in coal mines, Technics Technologies Education Management. 6, 861-865.

Vishal V., 2017. In-situ disposal of CO_2: Liquid and supercritical CO_2 permeability in coal at multiple down-hole stress conditions, Journal of CO_2 Utilization. 17, 235-242.

Wang H. Z., Li G.S., He Z. G., 2017. Mechanism study on rock breaking with supercritical CO_2 jet, Atomization and Sprays. 27(5), 383-394.

Wang Y.X., Mao D.B., Qi Q.X., 2003. Study on determining of mechanical parameters of rock mass used in numerical simulation, Journal of China Coal society. 28(6), 593-597.

White C.M., Smith H.D., Jones K.L., Goodman A.L., Jikich S.A., LaCount R.B., DuBose S.B., Ozdemir E., Morsi B.I., 2005. Sequestration of CO_2 in coal with enhanced coalbed methane recovery-A review, Energy & Fuels. 19(3), 659-724.

Wu F.P., Wei X.M., Chen Z.X., 2018. Numerical simulation and parametric analysis for designing high energy gas fracturing, Journal of Natural Gas Science and Engineering. 53, 218-236.

Xie H.P., Gao F., Zhou H.W., Cheng H.M., Zhou F.B., 2013. On theoretical and modeling approach to mining-enhanced permeability for simultaneous exploitation of coal and gas, Journal of China

Coal Society. 38(7), 1101-1108.

Yin G.Z., Jiang C.B., Wang J.G., Xu J., 2015. Geomechanical and flow properties of coal from loading axial stress and unloading confining pressure tests, International Journal of Rock Mechanics and Mining Sciences. 76, 155-161.

Zhang Y.B., Li E.Q., Liu J.W., Leng X.J., Li W.G., 2013. Applications of carbon dioxide cannon blasting on the problem of triangular flap top in coal mine handling mechanized mining face, Applied Mechanics and Materials. 256-259(PATR 1), 71-74.

Zhou F., Hussain Y., Cinar Y., 2013. Injecting pure N_2 and CO_2 to coal for enhanced coalbed methane: experimental observation and numerical simulation, International Journal of Coal Geology. 116, 53-62.

Highlights

1. A study on enhancing coal seam gas by cross-measure borehole using liquid CO_2 phase-transition blasting was conducted.

2. The fracture propagation in the coal seam after blasting was analysed by a numerical simulation.

3. There are 1.8–8 times increase in the efficiency of gas drainage following liquid CO_2 phase-transition blasting.

4. Observation holes surrounding the blast hole can increase the efficiency of enhancing coal seam gas using liquid CO_2 phase-transition blasting.